Development of an Infrared Diagnostic Instrument for the Measurement of CO_2 Isotope Ratios in Breath

CD Mansfield and HN Rutt
Infrared Science and Technology Group
Electronics & Computer Science Department
University of Southampton
Southampton
Hants. SO17 1BJ
UK

ABSTRACT

Stable CO_2 isotope breath tests are established as a valuable tool in diagnostic and investigative medicine. The instrument conventionally used is an Isotope Ratio Mass Spectrometer, however, the expense and complexity of such an instrument severely restricts the widespread and routine use of isotope tests. To realize their full potential an alternative instrument which is reliable, uncomplicated, insensitive to environmental and component fluctuations and affordable is required.

We present a system that satisfies these criteria using broadband non-dispersive infrared spectroscopy. Two isotopically distinct channel pathlengths are recorded for a basal and $^{13}CO_2$ enriched breath sample, the change in channel pathlength ratios required to restore transmitted intensity equilibrium between channels being related to the change in the $^{13}CO_2/^{12}CO_2$ concentration ratio. The novelty of the system lies in this negative feedback loop balancing the signal by means of adjusting one of the channels pathlength.

Results are presented proving the validity of using infrared spectroscopy for making such measurements without interference from breath trace compounds. Theoretical computer simulations using detailed modeling of CO_2 spectroscopy have been used to evaluate and quantify the risk posed to reliable measurement of $^{13}CO_2/^{12}CO_2$ due to various spectral effects. From this we have established operating tolerances necessary to avoid or limit the generation of a spurious result.

Keywords: Infrared spectroscopy, Carbon isotope ratio tests.

1. INTRODUCTION

The abundance of a breath trace compound's isotopic constituents can be used to perform controlled tests. Such tests are known as isotopic tracer tests and are realized by measuring the change in ratio of two isotopically distinct molecules, known as isotopomers, after a deliberate increase of the rarer isotopomer's concentration relative to a standard or basal level. This change is expressed as delta-values (δ ‰), the relative difference between the isotopic ratio of a breath sample after administration of a labeled dose and that of a baseline measurement. Delta values are calculated using equation (1), where Rs and Rr are the isotope ratios of an isotopically enriched breath sample and of a normal breath sample or reference source respectively.

$$\delta = \frac{Rs - Rr}{Rr} \times 1000 \qquad ‰ \qquad (1)$$

The first clinical breath tests were carried out in the sixties measuring expired $^{14}CO_2$. However, the utility of radioactive tracers has declined as the potential health risks associated with them have made it difficult to justify their use in clinical investigations along with problems due to strict regulations regarding permitted patient groups, disposal, shipment and security. As a consequence radioactive isotopes have largely been replaced with stable isotope tests. These incur greater costs but do not present any risk to health at the doses normally administered [1], have few restrictions on their use and do not exclude pregnant women or children from the advantages of isotope tracer tests.

Stable CO_2 isotope breath tests are now established as a valuable tool in diagnostic and investigative medicine with the potential to become more prominent in the future. Numerous ^{13}C-isotope ratio breath tests have been developed for the investigation of bacterial colonization, pharmacokinetics, gastrointestinal handling, liver function and other metabolic investigations [2-8], using an array of different ^{13}C substrates.

2 INFRARED ANALYSIS OF ISOTOPE RATIOS

A typical breath test may produce a response of 10-20 ‰ and Urea Breath Test protocols [9] use a delta-over-baseline value of just 5 ‰ to confirm the presence of Helicobacter Pylori. This represents a change in the $^{13}C^{16}O_2/^{12}C^{16}O_2$ ratio of approximately 0.005%, hence, any instrument used in isotopic breath tests has to be capable of detecting such small changes. The instrument conventionally used to measure the isotopic ratio of breath is an Isotope Ratio Mass Spectrometer (IRMS), a sensitive but expensive and complex instrument. As such, the widespread and routine use of isotope breath tests is severely limited, often being restricted to large research establishments and it is generally accepted that for isotope breath tests to realize their full potential a reliable, uncomplicated and affordable measuring system is required. It would therefore, be desirable for such a system to incorporate the following characteristics: low initial capital and maintenance costs; simplicity of use requiring no need for specialist operators; portability; highly specific to the quantity measured; and insensitive to component or environmental fluctuations.

To date the most promising alternative, offering relative simplicity and lower hardware costs, are those instruments that use non-dispersive IR spectroscopic methods, e.g. heterodyne [9] and optoacoustic spectroscopy [10]. These instruments give information regarding the total absorption over a certain wavenumber region, as opposed to the spectral profile of a sample and are more accurately described as IR ratiometers. We are therefore, developing an instrument that satisfies the above criteria using broadband non-dispersive IR spectroscopy. The basis of IR isotope ratio measurements is a characteristic of IR spectroscopy known as the isotope shift, the product of isotopic substitution which results in the separation of a vibrational mode's absorption band into its isotopic components. The most suitable CO_2 absorption band is the asymmetric stretching mode (ν_3) at 2350 cm^{-1} arising due to an excitation from the ground-state (00001) to the lowest energy excited state of this vibrational mode (00011). It is CO_2's strongest absorption band, displays an isotopic shift of 66 cm^{-1} between $^{12}C^{16}O_2$ and $^{13}C^{16}O_2$ (see Figure 1) and falls into a technologically accessible region of the spectrum.

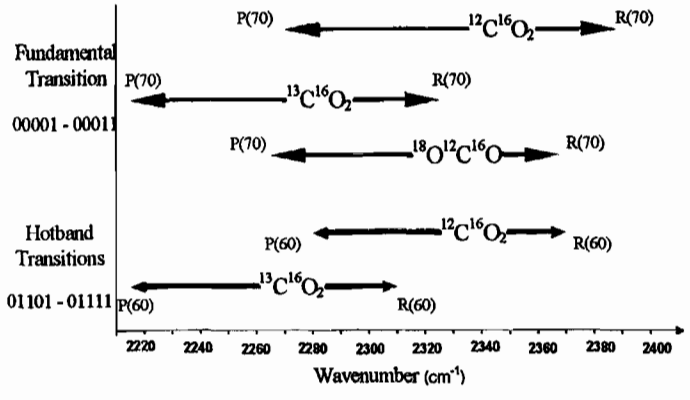

Figure 1 Absorption ranges of CO_2 isotopomer ν_3 fundamental transitions and hotbands.
AFGL (Airforce Geophysics Laboratory) energy level notation has been used [11].

3 RISK OF SPURIOUS RESULTS FROM COINCIDENT IR ABSORPTION BANDS

Use of IR spectroscopy raises the question of its validity as a reliable diagnostic technique due to the possibility of another absorbing Breath Trace Compound (BTC) possessing an absorption band that coincides with the spectrum of the two CO_2 isotopomers being measured. No corpus of high resolution IR absorption spectra for BTCs is available in the literature therefore, the authors compiled a list of over 230 trace compounds detected in breath including information on their origin, prevalence and concentration. A thorough evaluation of the literature on their IR absorption spectra enables identification of any IR absorption bands coincident with that of CO_2's ν_3 band [12] (see Table 1). Information was drawn from investigations considering the breath constituents of healthy subjects, compounds associated with various physiological disorders and exposure to industrial and environmental air contaminants. For the purpose of analysis these compounds were categorized into functional groups as this determines the basic structure of their spectrum hence, one can generalize upon the IR spectrum of members in a given group since one compound displays similar infrared absorption characteristics to its counterparts. Group classifications used in the Aldrich Infrared Spectra Library [13] have been adopted. Where a compound does not belong to a functional group, i.e. diatomic or triatomic compounds, they have been classified as inorganic. Summarizing this data we find the BTCs comprise of 31 functional groups of which around 40 % have been identified as metabolic products.

Table 1 Breath Trace Compounds with IR Absorption Bands lying in the 2400-2180 cm^{-1} Region.

BTC	IR Band Type	Functional Group
Acetonitrile	Fundamental	Non-aromatic Nitriles & Cumulated Double Bonds
Benzonitrile	Fundamental	Aromatic Nitriles & Cumulated Double Bonds
Nitrous Oxide	Fundamental	Inorganic
Carbon Monoxide	Fundamental	Inorganic
Hydrogen Sulfide	Fundamental	Inorganic
Ammonia	Combination	Inorganic
Water	Combination	Inorganic
Carbon Disulfide	Combination	Inorganic
Dimethyl Sulfoxide	Combination	Non Aromatic Sulfur-Oxygen Compounds
Benzene	Combination	Aromatic Hydrocarbon

Assuming that any system of detection is sensitive only to the frequencies at which CO_2 absorbs and has isolated the CO_2 ν_3 band, then the range of possible absorption line coincidence is approximately 2400-2180 cm^{-1}. BTCs with binary combination bands or minority isotopomers of BTCs would require concentrations equivalent to that of CO_2's to be of significance; of which there are none leaving just 5 out of over 230 breath trace compounds possessing fundamental absorption bands coincident with that of the CO_2 ν_3 band. Further consideration of these 5 coincident BTCs reveals that the CO band only partially overlaps, with the majority of line interaction being limited to very weak high J rotational lines. The other endogenous coincident BTC, H_2S, is limited to known population groups and has been detected in concentrations of only a few tens of parts per billion (ppb). Such concentrations are insignificant compared to that of $^{13}CO_2$ and therefore, do not pose a risk. The remaining 3 coincident BTCs are exogenous with N_2O being limited to post anesthesia whilst the others are of low occurrence and at concentration of ppb.

4 RISK OF SPURIOUS RESULTS FROM IR SPECTROSCOPIC EFFECTS

4.1 IR Spectroscopic Effects

The nature of diagnosis requires any instrument to be reliable and specific to the quantity of interest thereby, minimizing the risk of spurious results and a misdiagnosis. When designing an instrument for the IR measurement of CO_2 isotope ratios one should be conscious of several spectral effects that may be misinterpreted as changes in the isotope ratio, e.g. variation in the environmental conditions, a fluctuating source output or optical interference from the cell windows. Such effects may produce significant 'apparent' delta values, a negative or positive apparent delta leading to possible false negative or false positive diagnosis respectively.

4.1.1 Varying environmental conditions

Absorption line coincidence occurs between the isotopomers of CO_2 itself as the isotopic shift does not completely separate one isotopomer band from another. Considering the ν_3 fundamental absorption bands , Figure 1 $^{12}C^{16}O_2$ and $^{13}C^{16}O_2$ overlap between 2330 and 2230 cm^{-1} and both are coincident with the $^{12}C^{18}O^{16}O$ ν_3 band lying at approximately 2235-2376 cm^{-1}. Also there is coincidence with hotband transitions, produced by absorption from thermally excited states, which normally lie at a slightly lower wavenumber than the fundamental ν_3 transition. To create the two isotopically distinct channels cells containing either pure $^{12}CO_2$ or $^{13}CO_2$ are placed between the source and each sample cell, depending on which isotopomer is to be detected, at concentrations great enough to give zero transmittance over the frequencies they absorb. Any absorption bands not in close proximity to the CO_2 ν_3 band can be removed with conventional filters.

Variation in the degree of coincidence between sample and 'isotope filter' absorption lines may arise from a change in the rotational line intensity distribution or line-width being functions of temperature and pressure respectfully. Also the lower level thermal population of a hotband and thus, its total intensity varying dramatically with temperature. Hence, any change in transmittance brought about by fluctuations in temperature or pressure will be misinterpreted as a change in the $^{13}C^{16}O_2/^{12}C^{16}O_2$ ratio and since more than an hour may elapse between measurement of the reference (basal) ratio and subsequent sample ratios, conditions will almost certainly show some change without the use of rigid controls.

4.1.2 Multiple beam interference from IR windows

The materials used to manufacture IR windows have relatively large refractive indices and can act as low finesse etalons, producing spectral interference due to the transmitted ray undergoing repeated internal reflections between parallel surfaces of the window. Interference produces a variation of the transmitted intensity across the spectrum in which adjacent transmission peak separation, or free spectral range (FSR), and the modulation depth are determined by the window's refractive index and thickness. The multiple beam interference transmission can be described [14] by the formula

$$\frac{I_{(t)}}{I_{(i)}} = \frac{1}{1 + F \cdot \sin^2\left(\frac{\delta}{2}\right)} \tag{2}$$

where, $I_{(i)}$ is the incident intensity, $I_{(t)}$ is the transmitted intensity, δ is the phase difference and the coefficient F is equal to $4R / (1-R)^2$, R being the reflectivity.

The existence of etalon fringes does not necessarily present a problem as over a substantial bandwidth their intensities average to give the Fresnel transmission and thus, their effect assumed to be negligible however, if the spectrum of interest has rotational line separation similar or greater than that of the etalon this approximation does not hold. Such behaviour is attributable to a spectrum's total absorption being equal to the product of its component absorptions at a given wavenumber hence, it follows that total transmittance across the band differs depending upon the degree of rotational line and etalon fringe correlation. In the scenario of rotational line separation being similar or greater than etalon fringe

spacing a maximum modulation in integrated transmittance is observed as the etalon fringes move though 1 FSR, the greatest error over a bandwidth of several fringes being at equal spacing due to the number of interacting lines. This is the case for a typical window thickness of 2 mm, having a FSR of approximately 1.7-1.0 cm^{-1} depending upon the material's refractive index, and the CO_2 ν_3 mode having rotational line separation between the J(14) - J(16) lines, only even J lines being present, of approximately 1.7 and 1.4 cm^{-1} in the P-branch and R-branch respectively [12]. If the etalon spectrum remained constant then its influence is ratioed out against the background however, the fringes are not static with optical thickness being a function of temperature, expressed by

$$\frac{d(nl)}{dT} = n\frac{dl}{dT} + l\frac{dn}{dT} \tag{3}$$

where T is the temperature, n is the refractive index and l is the thickness of the window.

A change in temperature will result in the etalon spectrum being shifted slightly in wavelength and therefore, the background against which the sample spectrum is ratioed has substantially altered, leading to erroneous measurements of sample concentration. Characteristics of the etalon fringe pattern depend upon optical and thermal properties of the window (see Table 2) and its thickness. From these values and properties derived from them we have simulated the etalon fringes produced by different IR windows and their response to temperature change.

From Table 2 we see that the change in temperature required for the etalon to traverse through one FSR (T_{FSR}) is approximately 28 °C for CaF_2 falling to 6 °C for ZnSe. To avoid temperature sensitivity a value much less than T_{FSR} is required leading to a strong sensitivity in the zinc chalcogenide windows and a lesser but still significant sensitivity and each of the other window types.

Table 2. Optical and thermal properties [15] for common infrared materials @ 300 K and 4.3 μm. The etalon properties derived from them are for a typical window thickness of 2 mm and at normal incidence.

Window	n	α (x 10^{-6})	dn/dT (x 10^{-5})	R (%)	τ (%T)	T_{SUM} (%T)	Modulation Depth (%T)	d(nl)/dT (x 10^{-6})	FSR (cm^{-1})	TFSR (°C)
CaF_2	1.407	18.9	-0.75	2.86	89.19	94.44	10.81	5.73	1.78	28.15
NaCl	1.52	44.0	-3.23	4.26	84.33	91.83	15.67	1.04	1.64	15.54
KBr	1.535	38.5	- 3.8	4.45	83.67	91.47	16.33	6.33	1.63	25.48
Al_2O_3	1.664	5.6	1.37	6.21	77.97	88.30	22.03	6.91	1.50	23.35
ZnS	2.25	6.7	4.2	14.79	55.10	74.23	44.80	1.71	1.11	9.42
ZnSe	2.43	7.1	7.0	17.38	49.54	70.38	50.46	2.62	1.03	6.16

Where n is the refractive index, dn/dT the refractive index thermal coefficient and α is the linear expansion thermal coefficient. R is the single surface Fresnel reflectivity, from which we can calculate the window's transmission including multiple reflections incoherently summed, T_{SUM}. τ is the minimum etalon transmission and indicates the strength of fringe modulation, maximum etalon transmission being 100 %T. FSR is the resulting free spectral range and d(nl)/dT is the optical thickness thermal coefficient which leads to the temperature difference required to move the etalon through one complete spectral range, T_{FSR}.

4.1.3 IR source output variation

When source exitance is plotted against wavelength at various emitter temperatures a series of distribution curves, known as blackbody curves, are produced, each having a definite maximum which is shifted to shorter wavelengths and increases in output with rising temperature, the peak exitance occurring at 4.3 μm for a source temperature of 670 K. Thus, a fluctuation in source temperature results in a change of transmittance and since exitance is also wavelength dependent an apparent change in the $^{13}C^{16}O_2/^{12}C^{16}O_2$ ratio is observed. The extent of such variations will depend upon the stability of the source output and the blackbody curve profile across the region of interest, i.e. the source temperature.

4.1.4 Non-equivalent detector response

Detector responsivity is temperature dependent therefore, a change in the detector's operating temperature between measurement of the background and sample spectrum leads to a change in the corresponding responsivities, i.e. a non-equivalent response, and together with a wavelength dependence an apparent change in the $^{13}C^{16}O_2/^{12}C^{16}O_2$ ratio results. The effect can be severe for semiconductor based detectors but may be ignored when using pyroelectric detectors as these have a wavelength independent response, any change in channel responsivity being equal and thus, giving a zero delta value. Since pyroelectric detectors provide adequate performance for this application and are also cheaper and more convenient to use than semiconductor detectors the effect is not considered further.

4.2 Computer model

Since a combination of effects are likely to occur simultaneously in a system, leading to partial cancellation or reinforcement, erroneous results will appear transient in nature or go unnoticed, yet be serious in other circumstances. Modeling of the high resolution CO_2 spectrum together with simulation of the effect under investigation allow it to be studied in isolation, leading to the establishment of operating tolerances necessary to avoid or limit the generation of a spurious result.

4.2.1 CO_2 computer model

To investigate the implications such spectral effects have on the measurement of the $^{13}CO_2/^{12}CO_2$ ratio we have created a computer model of the ν_3 absorption band and fifteen of its most significant hotband transitions for the four main CO_2 isotopomer's, $^{12}C^{16}O_2$, $^{13}C^{16}O_2$, $^{18}O^{12}C^{16}O$ and $^{17}O^{12}C^{16}O$, requiring an accurate knowledge of CO_2 spectroscopy [16]. Line positions and energies are calculated with data on transition band centers, spectroscopic constants (B ,D and H), line broadening coefficients, partition sums, orbital angular momentum and Herman-Wallis coefficients taken from the Hitran database [11,17,18] (see Figure 2). Hitran is a comprehensive collection of spectroscopic parameters allowing the prediction of transmission through the atmosphere, CO_2 receiving thorough consideration, and is widely accepted as the standard reference. Close agreement exists between Hitran and our model values which serves to validate the accuracy of our simulations, e.g. rotational line transition energies typically display a 1 MHz deviation and line intensities an accuracy better than 0.1 % over J(0)-J(40), CO_2's strongest lines. Direct comparison with spectrum of known concentration, recorded using an FTIR spectrometer at 0.2 cm^{-1} resolution also confirm this.

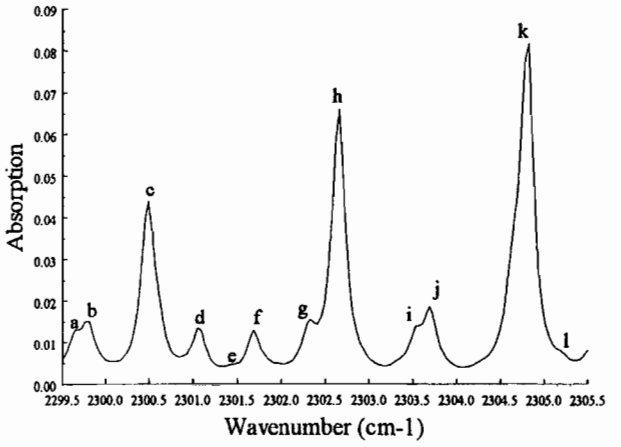

Rotational line assignment:

(a) $^{12}CO_2$ 01101-01111 P41; (b) $^{13}CO_2$ 00001-00011 R22;

(c) $^{12}CO_2$ 00001-00011 P52; (d) $^{13}CO_2$ 00001-00011 R24;

(e) $^{12}CO_2$ 10002-10012 P30; (f) $^{12}CO_2$ 01101-01111 P39;

(g) $^{13}CO_2$ 00001-00011 R26; (h) $^{12}CO_2$ 00001-00011 P50;

(i) $^{13}CO_2$ 00001-00011 R28; (j) $^{12}CO_2$ 01101-01111 P37;

(k) $^{12}CO_2$ 00001-00011 P48; (l) $^{12}CO_2$ 10002-10012 P26.

Figure 2. Detailed region of the computer generated CO_2 absorption spectrum.

Since a breath sample's CO_2 concentration and isotope abundance are significantly different from the atmosphere these values have been tailored to specifically simulate typical and limiting values in breath. Simulation of an instrument's operation involved the modeling of separate sample cells for the measurement of $^{13}CO_2$ and $^{12}CO_2$ with the relevant isotope filter cells. A sufficient level of wavelength selectivity is achieved by setting the isotope filter pathlength to 1.4 cm, removing the influence of corresponding rotational lines in the sample spectrum to approximately J(40) before line saturation breaks down, any residual line absorption being weak hence, cross interference is substantially reduced. Since the greatest operating pressure is expected to be 1050 mbar, filter pressure is also set to this ensuring the limiting value of rotational line width. Initial simulations encompassing the ν_3 transition up to J(80), i.e. 2267-2392 cm^{-1}, show that for a suitably strong absorption without line saturation a $^{12}CO_2$ sample cell pathlength of 1.0 mm is appropriate, giving transmittance of around 50 %T with the inclusion of isotope filters. The corresponding $^{13}CO_2$ sample cell pathlength for approximately equal absorption is 9.6 cm. Finally, we assume there is local thermal and pressure equilibrium between the channels. With such a model we are able to independently vary each cell's temperature, pressure and pathlength, the number of rotational lines and transitions to simulate, total CO_2 concentration, initial isotope abundance and change in the $^{13}CO_2/^{12}CO_2$ ratio. Results are in terms of integrated transmittance delta the desired concentration delta value being taken from a calculated calibration curve.

4.2.2 Simulations

Environmental change occurring over a typical breath test's duration are investigated by calculation of the apparent delta values generated across the conceivable range of temperature and pressure fluctuations, from an initial condition of Standard Temperature and Pressure (STP). Changes in pressure normally occur at approximately 1.0-1.5 mbar/hour however, in adverse weather conditions they have been recorded to change by as much as 6 mbar/hour [19]. It is assumed the instrument will be operated in a reasonably comfortable temperature environment, i.e. close to 25 °C, with a possible variation of 10 °C/hour due to changes in heating or ventilation. Also performing ratio measurements at altitude is investigated as many highly populated areas are several thousand feet above sea level, e.g. Mexico City, Mexico is at 7300 feet, lowering the standard pressure to approximately 750 mbar.

To evaluate apparent delta values induced by etalon temperature instability the spectrum of a typical breath's CO_2 sample was applied to the etalon fringe pattern (equation 2) of common IR window materials, with temperature varied across the range T_{FSR}. As the surfaces are of low reflectivity interference is produced substantially between only two beams. The sample and filter cell contents are assumed to remain at STP which of course will not be the case if there is a change in window temperature but is necessary to demonstrate the etalon's effect. In practice the variation in window temperature will be accompanied by a similar change in sample temperature, the combined effect being to reinforce or reduce the

etalon induced delta. Apparent delta values due to source output fluctuation are calculated by applying the source's blackbody output to the spectrum of a typical breath's CO_2 sample. Values calculated from fluctuations about the source's basal temperature give the temperature stability required to satisfy various apparent delta tolerance criteria. The sample cells are assumed to be stable at STP and a single source used thereby, eliminating temperature drift between channel sources.

4.3 Simulation results and discussion

We recall a typical diagnostic breath test yields a positive result for a delta of 5 ‰ furthermore, the natural fluctuation in a breath's $^{13}CO_2/^{12}CO_2$ ratio is between 0.4 ‰ [5] to 0.7 ‰ [20] with the minimum detectable change (2 S.D. definition) being 0.8 ‰ and 1.4 ‰ respectively. This sets a scale for the tolerance of any interfering effects.

4.3.1 Environmental conditions

Temperature and pressure tolerances for various apparent delta criteria are given in Table 3 and Figures 3a and 3b.

Pressure simulations reveal a linear relationship between sample cell pressure change and the resultant apparent delta value, with an increase in pressure giving a positive delta. Changes in pressure of 1 - 2 mbar produce an apparent delta value of less than ± 0.1 ‰ and in the extreme case of 6 mbar/hour the apparent delta is ± 0.3 ‰. Hence, the measurement is insensitive to fluctuations in environmental pressure and no control measures are required.

The relationship between fluctuation in gas cell temperature and the apparent delta value produced is linear over the range of environmental temperature change however, a strong temperature sensitivity is demonstrated, e.g. a change in temperature of less than 2 K results in an apparent delta value of 1 ‰. Thus, some form of temperature stabilization is necessary, a tolerance of ± 0.4 ‰ requiring the gas cell temperature to drift by no more than ± 0.7 K over the breath test's duration. Performing the measurement at altitude has no significant effect. Temperature sensitivity may also result from fluctuation between the filter and sample cells. Simulations of the filter cell temperature variation with respect to a stable sample cell at STP exhibit an even greater temperature sensitivity, a temperature drift of less than 0.5 K between the cells resulting in an apparent delta value of 1 ‰. Thus, if the filter and sample cell are not in thermal equilibrium it is necessary to stabilize the temperature of each gas cell to an accuracy of at least 0.2 K for a tolerance of ± 0.4 ‰.

Table 3. Gas cell temperature and pressure tolerances for various apparent delta criteria from basal condition of STP.

Apparent Delta Criteria (‰)	Temperature Change if Cells in Equilibrium (K)	Temperature Change of Filter Cell with respect to Sample Cell (K)	Pressure Change (mbar)
± 0.05			1
± 0.1	0.175	0.05	2
± 0.2	0.35	0.1	4
± 0.3	0.525	0.15	6
± 0.4	0.7	0.2	8
± 0.5	0.85	0.25	10
± 0.6	1.0	0.3	
± 0.7	1.19	0.35	
± 0.8	1.36	0.4	
± 1.0	1.7	0.45	
± 1.4	2.39	0.7	

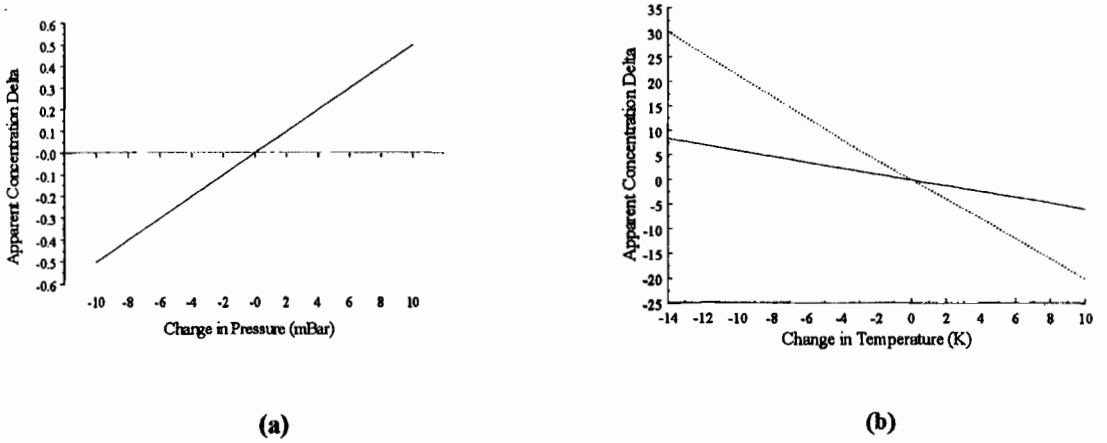

Figure 3. (a) Apparent delta values induced by fluctuations in sample pressure. (b) Apparent delta values produced from fluctuations in background temperature. The solid line shows temperature sensitivity for filter and sample cells in thermal equilibrium while the broken line is for filter cell temperature change relative to the sample cell.

4.3.2 Etalon fringes

The interaction between CO_2's absorption lines and the temperature sensitive etalon fringes result in large spurious delta values, see Table 4. The apparent delta value has a positive or negative contribution depending upon the window material, basal temperature and change in temperature having a greater affect on high index materials, see Figure 4.

The solution is simple as the maximum etalon fringe modulation is only obtained for plane-parallel windows, thus, to avoid instability windows should be manufactured with a deliberate wedge. Considering a single wavelength the inclusion of a wedge increases the transmitted ray's optical pathlength and therefore, phase difference as the wedge thickness increases across the aperture. This produces a set of Fizeau fringes across the window, each $\lambda/2$ increase in wedge thickness giving rise to another fringe. When a large number of fringes are produced the integrated transmittance across the aperture averages to give the incoherently summed transmittance, i.e. the effect of interference is removed.

To guarantee etalon fringes can not produce a significant error in delta the wedge angle must be large enough to produce a sufficient number of fringes, N, across the aperture at the longest wavelength of interest however, a larger wedge than required makes alignment more difficult due to unnecessarily large transmitted beam deviation. Calculation of delta with increasing window wedge thickness, $N\lambda/2$, indicates when the etalon fringe depth has diminished to a level which produces insignificant error. The corresponding wedge angle θ (in radians) for a given window of aperture a, refractive index n, and at wavelength λ, is given by $\theta = N\lambda / 2na$, where N is the number of fringes across the aperture. Hence, a 25 mm diameter window requires a wedge angle of 2.2 mrad. (7.6 minutes of arc) for ZnSe and 0.8 mrad. (2.75 minutes of arc) for CaF_2 to give an apparent delta of less than 0.1 ‰ across the temperature range T_{FSR}. This corresponds to a value of approximately N=50 for the zinc chalcogenides down to approximately N=10 for lower refractive index materials such as fluorides. Thus, it is necessary to purchase any windows with a wedge of at least this magnitude, standard windows often being too parallel to assure the elimination of etalon fringe effects.

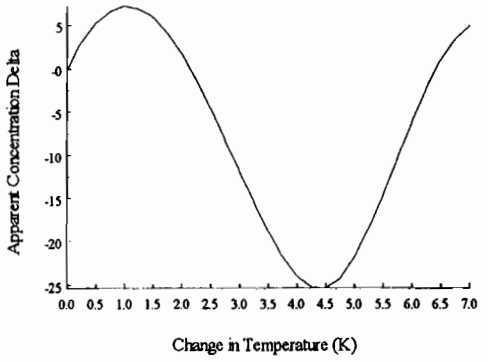

Figure 4. Apparent delta value induced by etalon fringes of a 2.0 mm thick ZnSe window and CO_2.

Table 4. Modulation in apparent delta as etalon fringe moves through 1 FSR with temperature change, T_{FSR}.

IR Material	T_{FSR} (°C)	Modulation (‰)
CaF_2	28.15	4.8
NaCl	15.54	4.8
KBr	25.48	14.7
Al_2O_3	23.35	13.4
ZnS	9.42	30.8
ZnSe	6.16	32.5

4.3.3 Source output

Fluctuations in source output vary linearly with the apparent delta value produced, an increase in source temperature leading to a positive delta value, i.e. exitance of the $^{13}CO_2$ channel has increased by a greater proportion than that of the $^{12}CO_2$ channel, and vice versa. The magnitude of this temperature sensitivity depends upon the source's operating temperature, however a change of 1 K will produce a significant apparent delta value over the range of 400-1200 K. The temperature stability required to satisfy various apparent delta tolerance criteria is shown in Figure 5.

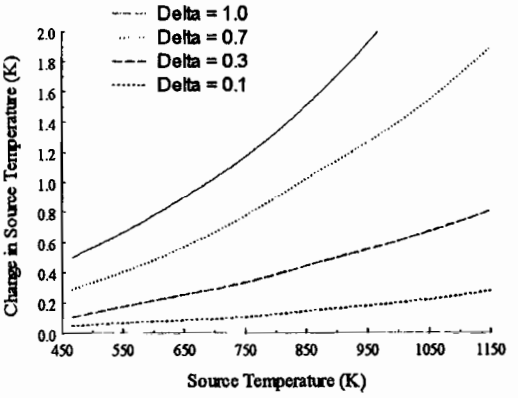

Figure 5. Source temperature fluctuation tolerances for various apparent delta criteria

Since isotope ratio tests are concerned with measuring relative changes in isotopomer abundance the delta response is related to the relative change in channel exitance due to a change in temperature, non-zero delta values being attributable to channel wavelength separation resulting in interaction at different points of the blackbody curve. Analytically this can be expressed as the cross derivative: $\frac{\partial}{\partial T} \cdot \left[\frac{1}{M} \cdot \frac{\partial M}{\partial \lambda} \right]$.

It is observed that sensitivity falls with increasing source temperature implying the use of temperatures in excess of the 4.3 μm peak exitance blackbody curve. However, a source operating at 1000 K may still only fluctuate by 0.2 K, equivalent to a 1 mm^2 emitter's output varying in irradiance by ± 0.045 mW , for a ± 0.1 ‰ tolerance. Very accurate stabilization of the source's power supply and thermal environment is required.

5 INSTRUMENT DESIGN

The design of our non-dispersive IR CO_2 isotope ratio breath analyzer can be seen in Figure 6. IR radiation from an appropriate broad band source is divided into two paths after passing through a suitable interference filter to isolate the range of wavelengths encompassing the CO_2 ν_3 mode. Selectivity is further enhanced by placing cells containing either pure $^{12}CO_2$ or $^{13}CO_2$ in each path, depending on which isotopomer is to be detected. The concentration of these 'isotopic filters' should be sufficient to give zero transmittance over the frequencies they absorb thereby, creating two isotopically distinct channels. Two breath sample cells are placed in the beams and are mounted in close proximity to one another so that they may communicate directly, giving thermal and pressure equilibrium between channels. For the condition of equal transmitted intensities these cells require lengths approximately in the ratio of the ^{12}C:^{13}C isotopic abundance, i.e. 90:1. The longer cell is placed in the beam path that interacts with the rarer isotopomer of $^{13}CO_2$ and is of adjustable length by some electrical means, whilst the second, shorter cell is placed in the $^{12}CO_2$ channel and has a fixed pathlength. The two IR beams are combined onto a single detector using the necessary optics.

Output from the IR detector is processed with a phase sensitive detector (PSD) whose reference signal is derived from a chopper positioned between the source and sample cells in such a way that each beam path is alternately open and obscured. If the transmitted IR intensity is the same from each channel no signal will be produced, whereas if the intensities are unequal a positive or negative output signal is produced. The signal from the PSD is used to adjust the variable length cell in such a way as to reduce the output of the detector to zero. The system constitutes a feedback loop. Thus, in practice channel pathlengths are recorded for a basal and $^{13}CO_2$ enriched breath sample, the change in channel pathlength ratios required to restore transmitted intensity equilibrium between channels, resulting from the action of an actuator-feedback loop, being a direct measurement of changes in the $^{13}CO_2/^{12}CO_2$ concentration ratio. Calibrated may be performed by using gases of previously measured composition.

The system's novelty lies in its use of this negative feedback and balancing of the signal by pathlength adjustment, the only change registered being that in the relative intensities of the two isotopomer channels.

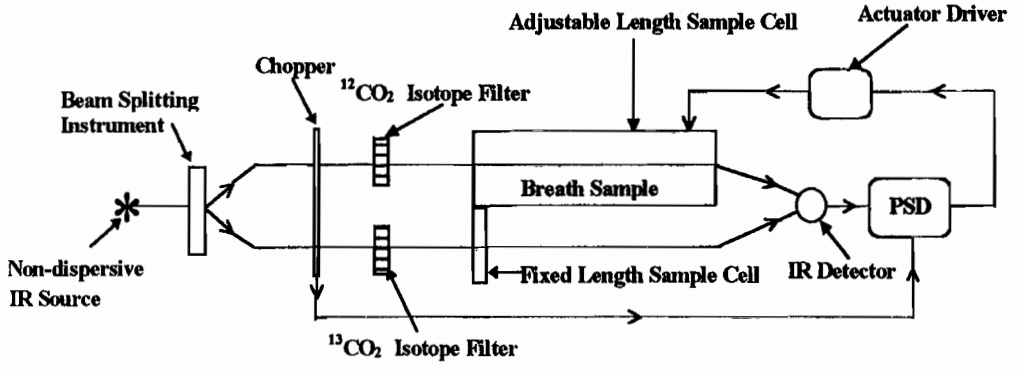

Figure 6. Schematic drawing of the infrared CO_2 isotope ratio breath analyser.

6 CONCLUSIONS

Through evaluation of the literature on BTCs and their IR absorption spectra we find only 5 out of over 200 compounds detected in the breath have absorption bands coincident with that of the CO_2 ν_3 band. However, none of these pose a risk of spurious results so we conclude the $^{13}C^{16}O_2/^{12}C^{16}O_2$ ratio can confidently be measured using an instrument based on IR absorption without risk of interference from other BTCs, provided the infrared window used is restricted to 2400 - 2180 cm^{-1}. This is based upon the innate scarcity of fundamental IR absorption bands in the 4.3 μm region, leading to virtual isolation of the CO_2 ν_3 band from any other BTC's absorption band.

Various spectral effects associated with instruments using non-dispersive IR spectroscopic methods have been identified and the risk these pose to reliable measurement of $^{13}CO_2/^{12}CO_2$ ratios quantified. We have demonstrated the $^{13}CO_2/^{12}CO_2$ ratio measurement's temperature sensitivity due to spectral interference from window etalon effects, changes in environmental condition and fluctuation of source output. Unless appropriate measures to control or compensate for these effects are implemented temperature variations well within typical laboratory fluctuations will lead to spurious delta values. From the preceding analysis we have established operating tolerances necessary to avoid or limit the generation of a spurious result due to spectral effects, within the bounds of conceivable operating conditions. Hence, for reliable measurement of $^{13}CO_2/^{12}CO_2$ ratios using IR spectroscopy etalon effects are eliminated using windows wedged at a minimum angle of 0.8-2.2 mrad. depending on the material. The source and sample cells require temperature stabilization, a fluctuation of 0.2 K resulting in an apparent delta of ± 0.1 ‰ and ± 0.4 ‰ respectively. Ambient pressure changes and operation at altitude exhibit insignificant delta values requiring no controls.

Following these operating tolerances our system has the advantage of being insensitive to fluctuations in gas cell pressure or temperature, non-linearity in IR detector sensitivity or IR source output and since the system is AC coupled DC drift effects are eliminated except at the output of the PSD. Furthermore, the systems balancing nature will measure changes in the relative concentrations of each isotopomer and not their absolute concentrations making it insensitive to the actual percentage of CO_2 in the sample, providing it is stable during the test.

The principle of using IR radiation to measure the composition of a gas mixture and the application of 'correlation' filters to isolate the appropriate wavelengths is well known. However, to our knowledge the balanced nature of the system using adjustable pathlength cells driven by a actuator-feedback loop is entirely novel. It has numerous practical advantages and is the key to the required low cost, high accuracy instrument. Using the results obtained from these and further unreported simulations a prototype instrument is now under construction.

REFERENCES

1. Keller U and Rennie MJ "Stable Isotopes in Clinical Research" *European Journal of Clinical Investigation* **16** pp. 97 - 100, 1986

2. Lown KS, Thummel KE, Benedict PE, Shen DD, Turgeon DK, Berent S and Watkins PB "The Erythromycin Breath Test Predicts the Clearance of Midazolam." *Clinical Pharmacology and Therapeutics* **57** pp. 16-24, 1995

3. Duan LP, Braden B, Caspary WF and Lembcke B "Influence of Cisapride on Gastric Emptying of Solids and Liquids Monitored by ^{13}C Breath Tests." *Digestive Diseases and Sciences* **40** pp. 2200-2206, 1995

4. Watkins JB, Schoeller DA, Klein PD, Ott DG, Newcomer AD and Hofmann AF "^{13}C Trioctanoin: A Non-radioactive Breath Test to Detect Fat Malabsorption." *J. Lab. Clin. Med.* **90** pp. 422-430, 1977

5. Dewit O, Prentice A, Coward WA and Weaver LT "Starch Digestion in Young Children with Cystic Fibrosis Measured Using a ^{13}C Breath Test." *Pediatric Research* **32** pp. 45-49, 1992

6. Mion F, Queneau PE, Rousseau M, Brazier JL, Paliard P and Minaire Y "Aminopyrine Breath Test: Development of a ^{13}C Breath Best for Quantitative Assessment of Liver Function in Humans." *Hepto-Gastroenterology* **42** pp 931-938 1995

7. Witschi A, Mossi Sandro, Meyer B, Junker E and Lauterburg B "Mitochondrial Function Reflection by the Decarboxylation of ^{13}C Ketoisocaproate Is Impaired in Alcoholics" *Alcoholism: Clinical Experimental Research* **18** pp. 951-955, 1994

8. Koletzko S, Haisch M, Seeboth I, Braden B, Hengels K, Koletzko B and Hering P "Isotope Selective Non-dispersive IR Spectrometry for Detection of Helicobacter Pylori Infection with ^{13}C-Urea Breath Best." *Lancet* **345** pp. 961-962, 1995

9. Irving CS, Klein PD, Navratil PR and Boutton TW "Measurement of $^{13}CO_2/^{12}CO_2$ Abundance by Nondispersive IR Heterodyne Ratiometry as an Alternative to Gas Isotope Ratio Mass Spectrometry." *Anal. Chem* **58** pp. 2172-2178, 1986

10. Braden B, Haisch M, Duan LP, Lembcke B, Caspary WF and Hering P "Clinical Feasible Stable Isotope Technique at a Reasonable Price: Analysis of $^{13}CO_2/^{12}CO_2$ Abundance in Breath Samples With a New Isotope Selective Nondispersive Infrared Spectrometer." *Z Gastroenterol* **32** pp. 675-678, 1994

11. Rothman LS *Hitran96 Molecular Database CD-ROM* 1996 (North Andover: Ontar Corporation) 1996

12. C D Mansfield and H N Rutt "The Application of Infrared Spectroscopy to Breath CO_2 Isotope Ratio Measurements and the Risk of Spurious Results" *Physics in Medicine and Biology* **43** pp. 1225-1239, 1998

13. Pouchert C J *The Aldrich Library of Infrared Spectra 3rd Ed.* (Milwaukee: Aldrich Chemical Co.) 1981

14. Born M and Wolf E *Principles of Optics 3rd ed.* (Pergammon Press, London) pp.323 - 329, 1965

15. Klocek P *Handbook of Infrared Optical Materials* (Marcel Dekker, New York) 1991

16. Herzberg G *Molecular Spectra and Molecular Structure Vol. II Infrared and Raman Spectra of Polyatomic Molecule* (New York: D.Van Nostrand Co., Inc.) p 272-369, 1945

17. Rothman LS, Gamache RR *et al* "The Hitran Molecular Database: Editions of 1991 and 1992." *J. Quant. Spectrosc. Radiat. Transfer* **48** pp 469 - 507, 1992

18. Rothman LS, Hawkins RL, Wattson RB and Gamache RR "Energy Levels, Intensities, and Linewidths of Atmospheric Carbon Dioxide Bands." *J. Quant. Spectrosc. Radiat. Transfer* **48** pp 537 - 566, 1992

19. Hardy DC *UK Meteorological Office, private communication,* 1996

20. Schoeller DA, Klein PD, Watkins JB, Hiem T and MacLean Jr. WC "^{13}C Abundance of Nutrients and the Effect of Variations in ^{13}C Isotopic Abundance of Test Meals Formulated for $^{13}CO_2$ Breath Tests." *The American Journal of Clinical Nutrition* **330** pp. 2375-2385, 1980